Proceedings of the XVII ECSMGE-2019
Geotechnical Engineering foundation of the future
ISBN 978-0-7277-6067-8

doi: 17ecsmge-2019-Y-XXXX

XVII European Conference
ECSMGE 2019
Reykjavík
on Soil Mechanics
and Geotechnical Engineering

Theoretical and experimental investigation of the multiaxial soil response around monopile foundations

Etude théorique et expérimentale de la résponse multiaxiale des sols autour des fondations monopiles

A. Mandolini
Horizon Geosciences Ltd, Bristol, UK, formerly University of Bristol, Bristol, UK

A. Diambra, E. Ibraim
University of Bristol, Bristol, UK

ABSTRACT:
Large diameter monopiles are still the preferred foundation method for offshore wind farm developments. The performance of the pile under cyclic lateral load is the leading design criterion for this foundation option. In order to investigate the cyclic response of the soil surrounding the pile, it is simplistically assumed that soil elements located in the direction of pile loading are subjected to axisymmetric triaxial loading, while those on the side of the pile are subjected to simple shear loading conditions. Conversely, by setting up a 3-D finite element analysis for a hollow cylinder driven pile, this paper will investigate the real multiaxial (6-D) stress paths induced in soil elements around the pile. It will be shown how the stress paths change according to (*i*) the orientation of the soil element with respect to the pile loading direction, (*ii*) the depth of the soil element from the ground surface and (*iii*) the lateral distance of the soil element from the pile. It will be found that most of the soil elements (even those in front and on the side of the pile) will follow a multiaxial stress path, with continuous orientation of principal stress axis. This research will then develop guidance on which experimental apparatus and loading conditions can be imposed to satisfactorily approximate the loading history experienced by each soil element. Differently from common practice, the necessity of using multiaxial stress equipment (e.g. the hollow cylinder torsional apparatus) will be demonstrated. Examples of real experimental tests and test results under the loading conditions representative of laterally loaded pile will be also shown.

RÉSUMÉ:
Les monopiles de grand diamètre constituent toujours la méthode de base privilégiée pour le développement de parcs éoliens offshore. La performance du pieu sous une charge latérale cyclique est le critère de conception principal pour cette option de fondation. Pour étudier la réponse cyclique du sol entourant le pieu, on suppose simplement que les éléments du sol situés dans la direction du chargement du pieu sont soumis à un chargement axisymétrique triaxial, tandis que ceux situés à côté du pieu sont soumis à des conditions de chargement par cisaillement simples. Inversement, en établissant une analyse par éléments finis 3D pour un pieu entraîné par un cylindre creux, cet article étudiera les chemins de contrainte multiaxiaux (6D) réels induits dans les éléments de sol autour du pieu. Nous démontrerons comment les chemins de contrainte changent en fonction de (i) l'orientation de l'élément du sol par rapport à la direction du chargement du pieu, (ii) la profondeur de l'élément du sol par rapport à la surface du sol et (iii) la distance latérale de l'élément du sol de la pile. On constatera que la plupart

des éléments du sol (même ceux situés à l'avant et aux côtés du pieu) suivront des chemins de contraintes multiaxiales, avec une orientation alignée avec l'axe de contrainte principale. Cette recherche développera ensuite des orientations sur les appareils expérimentaux et les conditions de chargement pouvant être imposés pour obtenir une approximation satisfaisante de l'historique du chargement subi par chaque élément du sol. Contrairement à la pratique courante, la nécessité d'utiliser un équipement de contrainte multiaxial (par exemple l'appareil torique à cylindre creux) sera démontrée. Des exemples d'essais expérimentaux réels et de résultats d'essais dans des conditions de chargement représentatives d'un pieu chargé latéralement seront également présentés.

Keywords: Multiaxial stress; Sands; Cyclic loading; Hollow cylinder Torsional apparatus.

1 INTRODUCTION

The offshore wind market registered globally the highest growth during recent years. The UK, in particular, is set to double its capacity over the next decade and the offshore wind energy will soon be able to provide over the 30% of the country's required electricity (EWEA, 2015).

The design of the Offshore Wind Turbine (OWT) foundation poses a new set of geotechnical engineering challenges from the combination of significant cyclic moments and lateral loads imposed by the loads on the superstructure. Furthermore, throughout its design life, the OWT foundation is subjected to millions of cyclic loading ($>10^8$) arising from wind, sea waves, rotor dynamics (known as 1P) and blade shadowing effects (2P or 3P). Each contribution is unique in terms of magnitude, frequency and number of cycles and, in addition, it is three-directional by nature (Nikitas et al. 2016). The serviceability state of OWT monopiles is still uncertain as the long-term response of the ground around the monopile shaft is not yet well-understood. Many authors (Achmus et al. 2009; Leblanc et al. 2010, among others) raised the issue of fatigue damage caused by an accumulation of pile head rotation under the application a large number of lateral loads and overturning moments. On the other hand, OWT's are dynamically sensitive structures and their natural frequency response relies heavily on the stiffness of the soil surrounding the foundation. A change of the soil stiffness under the prolonged action of cyclic loadings may shift the system excitations towards the structural resonance frequencies leading to a dangerous amplification of the dynamic loads which could jeopardize the serviceability of the turbine.

This paper presents a theoretical analysis by means of a three-dimensional finite element model of a large diameter monopile foundation in granular material. The model has been developed to understand the stress paths induced in typical soil elements adjacent to the pile during loading. The numerical results were used to guide the experimental programme carried with the Hollow Cylinder Torsional Apparatus (HCTA) to investigate the long-term evolution of soil stiffness which may affect the dynamic properties of a wind turbine, under low amplitude high-cyclic loading. The HCTA was equipped with a complex local strain measurement system formed by six non-contact sensors able to precisely measure changes of the elastic properties of the material.

2 NUMERICAL INVESTIGATION

2.1 Numerical Model

Numerical modelling methods are regularly employed in offshore engineering because they provide an efficient and convenient approach to determine the response of soil surrounding deep foundations. A three-dimensional finite element analysis was carried out to understand the mechanisms developed in terms of load time history

and stress path in the soil. The model simulates a large monopile foundation embedded in homogenous sand subjected to lateral loading at the seabed level. The model main dimensions, shown in Figure 1, comprise a pile diameter (*Dp*) of 10 m and an overall pile length (*Lp*) of 60 m (6*Dp*), half of which embedded into the seabed (*Le*). This geometry reflected the slenderness ratios (*Lp/Dp*) used in typical OWT and in other similar numerical analyses (Achmus et al., 2009). The soil domain was modelled with a typical circular shape with a width of 11*Dp* (*Ds*), and height of 5*Dp* (*Ls*), which leaves 20 m (0.67*Lp*) from the pile toe to the bottom boundary. Distant boundary conditions were imposed in order to eliminate the influence of the boundary effect on the simulations (Abdel-Rahman & Achmus, 2005).

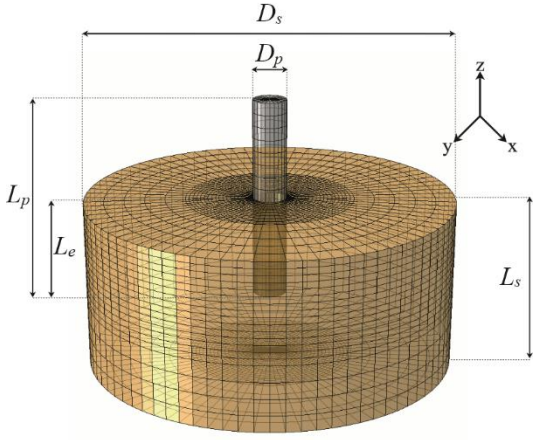

Figure 1. Three-dimensional FE model, geometry of the pile and soil domain.

The pile was made of steel with a stiffness and a length/diameter ratio typical of a rigid body which rotates as a unit. The granular soil behaviour was analysed using linear-perfectly plastic model. The geotechnical properties of the sand, listed in Table 1, relate closely to the actual properties of the Hostun sand (Mandolini et al, 2018).

The numerical analysis is divided into three main stages: (*i*) the application of the geostatic pressure, (*ii*) the "installation" of the pile and (*iii*) the application of horizontal/vertical load at ground level. To obtain a 3D view of soil behaviour around the pile shaft, several mesh elements were selected at a different depth, distance and orientation from the pile wall. The principal stresses were derived by the stress matrixes of the selected mesh elements, then compared between the three loading stages.

Table 1. Soil parameters for elasto-plastic analysis

Elastic		**Mohr-Coulomb plasticity**	
Young's modulus E_s	45 MPa	Friction angles (φ')	35°
Poisson Ratio	0.35	Dilatancy (ψ)	10°
Unit weight (γ_s)	1600 kg/m^3	Cohesion* (c')	0.1 kPa

* c'=0.1 kPa was necessary to find the convergence of the solution

2.2 Numerical results

The analysis of the stress paths for the selected soil elements concentrates mostly on the application of the horizontal load stage. The evolution of the direction of the principal stress axes during this stage of loading is shown in Figures 2, where the x-axis is the radial direction from the pile centre and the z-axis is the vertical axis. For a soil element in front of the pile (A=0°, where A indicates the orientation of the soil element from the direction of the load application) the rotation of two principal stress axes can be observed (Figure 2a). For soil elements oriented at A=45° and A=90°, all the principal stress axes re-orientate during loading (Figures 2b and 2c).

The results on the whole FE mesh showed that the rotation of principal stresses (σ_1, σ_2 and σ_3) almost invariably occur within the surrounding soil of the foundations (Figure 3). Blue and green soil elements, in Figure 3, were subjected to two or three rotations of the principal stress direction respectively. In the direction of the horizontal load (A=0°), an estimation of up to 85% of the mesh elements suffered rotation of two principal stress axes. Due to symmetry, elements on the A=0° direction should not experience rotation of all three principal stress axes and the appearance of some green elements is due to small numerical

inaccuracies in the superficial elements or those in close contact with the pile. The combined loads applied on the pile head do not impose any changes in the stress path direction for the remaining selection of mesh elements (red domain in Figure 3), due to low-stress levels in these elements.

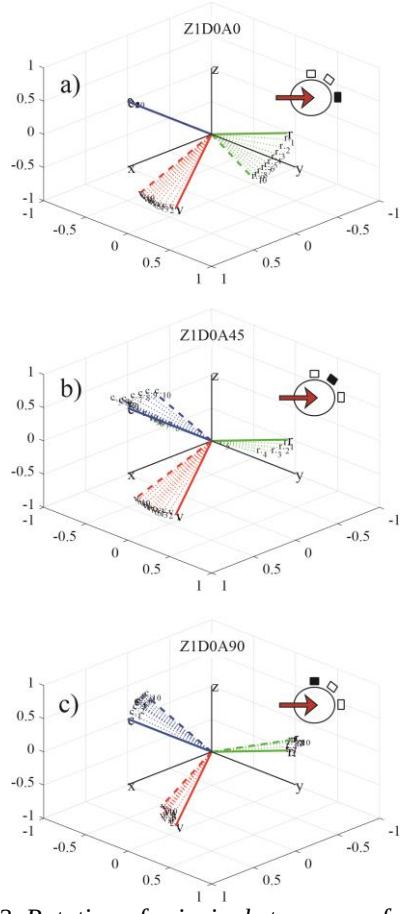

Figure 2. Rotation of principal stress axes for typical soil elements during laterally loading of a pile: (a) in front of the pile (A=0°); (b) at 45° from load direction (A=45°); (c) perpendicular to load direction (A=90°).

The conditions identified on the elements subjected to exclusively two rotations of the principal stress axes (blue elements in Figure 2) can be replicated in a laboratory by using the HCTA, which possesses the capability of testing in multiaxial conditions. The next part of this research aims to investigate how the long-term cyclic rotation of principal stress axes can affect the small strain stiffness of granular soils.

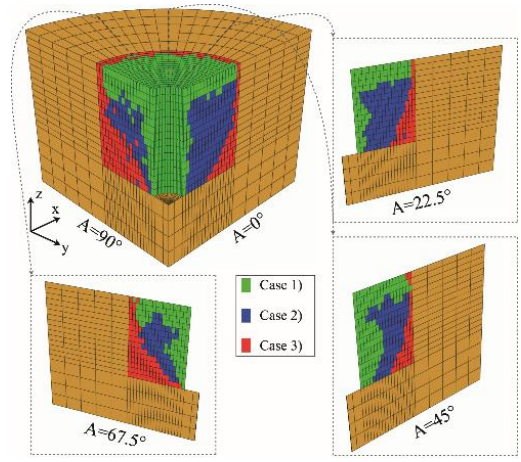

Figure 3. Schematic view of the elements surrounding the model. Case 1) rotation of all three stress principal axes, Case 2) rotation of two stress principal axes, Case 3) no rotation.

3 MATERIAL

Hostun RF (S28) sand has a high siliceous content (SiO_2 > 98%), angular to subangular grains, a mean grain size (D_{50}) of 0.32mm, specific gravity (G_s) of 2.65 and minimum and maximum void ratio (e_{min} and e_{max}) of 0.62 and 1.00. The particle size distribution is shown in Figure 4.

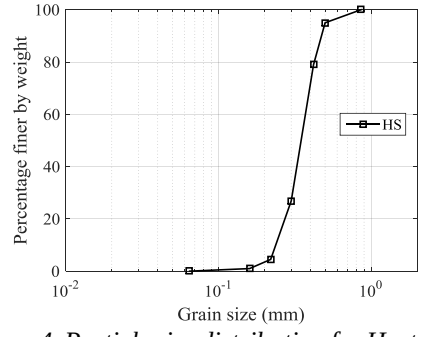

Figure 4. Particle size distribution for Hostun sand.

4 TESTING EQUIPMENT

The HCTA has the capability to independently govern axial load (*W*), torque load (*T*) and internal and external pressure (*Pi* and *Po*) on a typical hollow cylindrical shape sample (Figure 5a). The application of these enables the control of most the components of the stress matrix: axial (σ_z), radial (σ_r), circumferential (σ_θ) and shear stress ($\tau_{\theta z} = \tau_{z\theta}$) on an element of the hollow cylindrical specimen (Figure 5b). Equations for stress and strain components of hollow cylinder specimens are provided by Hight et al. (1983).

The stress path can be characterised by four independent parameters, such as the mean principal effective stress *p* (1), generalised deviatoric component of stress *q* (2), intermediate principal stress parameter *b* (3) and the angle α_σ (4) between the major principal stress σ_1 and the vertical direction (Figure 5c), defined as:

$$p' = \frac{\sigma_z+\sigma_\theta+\sigma_r}{3} = \frac{\sigma_1+\sigma_2+\sigma_3}{3} \quad (1)$$

$$q = \sqrt{\frac{(\sigma_z-\sigma_r)^2+(\sigma_r-\sigma_\theta)^2+(\sigma_\theta-\sigma_z)^2}{2} + 3{\tau_{\theta z}}^2} \quad (2)$$

$$b = \frac{\sigma_2-\sigma_3}{\sigma_1-\sigma_3} \quad (3)$$

$$\alpha_\sigma = \frac{1}{2}\, tan^{-1}\left(\frac{2\tau_{\theta z}}{\sigma_z-\sigma_\theta}\right) \quad (4)$$

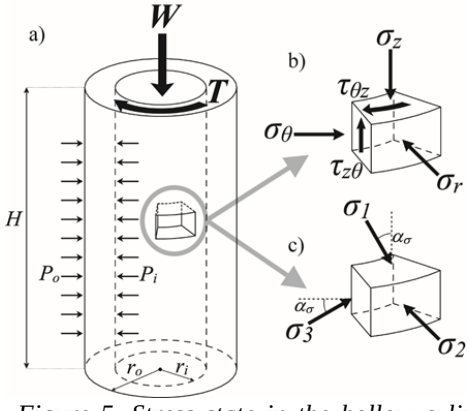

Figure 5. Stress state in the hollow cylinder torsional sample (a). Details of the element in the wall: the stress components (b) and main principal stresses directions (c).

5 SMALL STRAIN MEASUREMENTS

The HCTA is equipped with a complex system of six non-contact transducers with the aim to provide access to the soil stiffness including its evolution with the general strain and stress levels.

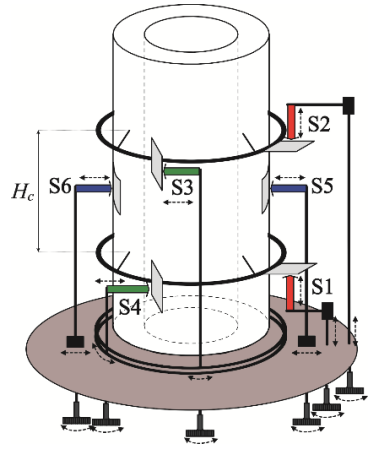

Figure 6 Schematic representation of the strain measurement system.

All six sensors were designed to move independently in order to allow small adjustments of their position during the test. The targets, towards which the sensors were aiming, were instead fixed with the sample (Figure 6). The six non-contact transducers enable the precise measurement of the strain developing in the central part of the sample.

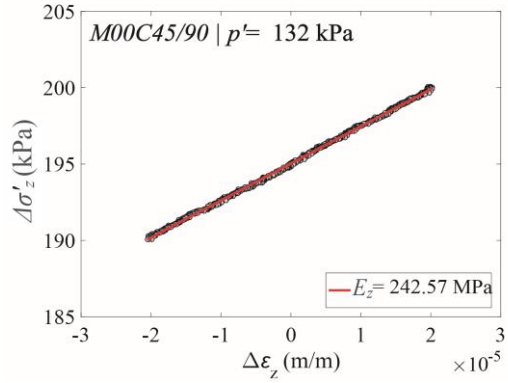

Figure 7 Example of load/unload cycle to evaluate the sample stiffness.

Young's and shear moduli (E_z and $G_{\theta z}$, respectively) were determined at investigation points throughout the test, where the sample was subjected to a few very small (elastic range) compressional and torsional unload/reload loops. The small strain stiffness was then evaluated by linear regression of the stress and strain relationship (an example is shown in Figure 7).

6 SAMPLE PREPARATION

The main dimensions of the prepared samples are shown in Figure. 5a: outer radius (r_o) of 50mm, inner radius (r_i) of 30mm and 200mm height (H).

Typically, the sample fabrication procedure involves the deposition of oven-dried sand within an inner and an outer mould. The sand was gently poured maintaining a constant zero fall height. In order to achieve the target density, a light vertical vibration (55Hz) was applied through a small shaking table. Once the sample was sealed within the top and bottom caps, it was transferred inside the triaxial cell and the small strain measuring system was set up around it.

The samples were prepared for testing in fully saturated conditions which were ensured by CO_2 flushing method together with employment of water back pressure up to 300 kPa. All the tests were carried out in drained conditions, under the same effective confinement pressure of 100 kPa and with an initial void ratio of about 0.82.

7 EXPERIMENTAL PROGRAMME

The testing strategy was designed to simulate the long-term response of medium-dense samples after the application of a large number of multiaxial cyclic loading in drained conditions. As shown in Figure 8, the soil was first consolidated to deviatoric stress level (q_{ave}) in the $\tau_{\theta z}/p'$ vs σ_z-$\sigma_\theta/2p'$stress plane at a direction $\alpha_{\sigma,m}$, and then subjected to long-term cyclic loading of amplitude $\tau_{\theta z,amp}$ and direction $\alpha_{\sigma,c}$.

Cycles were applied at the same loading frequency of 0.05Hz, while the amplitude of the torsional cycles changed between $\tau_{\theta z,amp}$= ±3, ±5 and ±12 kPa. Small strain stiffness checks were carried out periodically imposing small axial or torsional cycles. Periodically the sample was subjected to large unloading-reloading loops to simulate a storm loading event between cyclic batches (Figure 9).

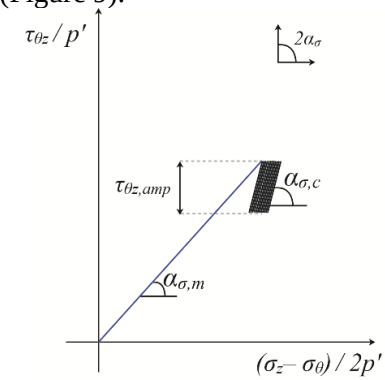

Figure 8 Schematic representation of $\alpha_{\sigma,m}$ and $\alpha_{\sigma,c}$ in the normalised deviatoric-tangential stress plane

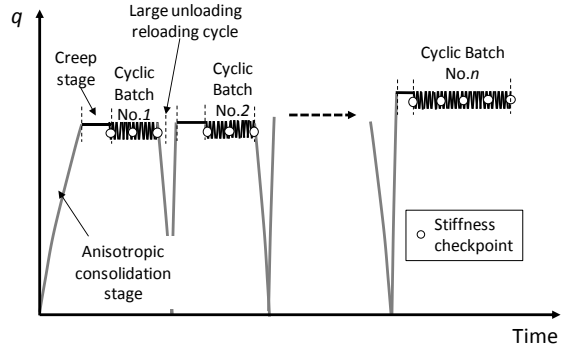

Figure 9 Investigation points and unloading-reloading loop between cyclic batches (B_i)

Two selected tests will be presented here, *M00C45/90* and *M00C45H*. Both were pre-stressed in $\alpha_{\sigma,m}$=0º (axial) direction to simulate elements in front of the pile and then subjected to torsional cyclic loading $\alpha_{\sigma,c}$=45º. For comparison, some cyclic loading batches for test *M00C45/90* were performed imposing $\alpha_{\sigma,c}$=0º and 90º (compression and extension) directions and a few batches were performed at double deviatoric stress level ($q_{ave2} = 2q_{ave1}$).

The torsional cyclic loading in test *M00C45H* was performed exclusively at the highest deviatoric stress level, q_{ave2} corresponding to a mobilised friction angle of *29.1°*. The main features including the number of cycles involved are listed in Table 2.

Table 2 List of tests presented, e_0 stands for initial void ratio and φ'_m mobilised effective friction angle.

Name	e_0	$2\alpha_{\sigma,c}$	φ'_m	No. cycles
M00C45/90	0.807	±45°, 0°,90°	18.8°, 29.1°	670005
M00C45H	0.828	0°	29.1°	145440

8 TEST RESULTS

For the first half of the test *M00C45/*90, the sample was subjected to $3 \cdot 10^5$ small torsional cyclic loading ($\tau_{\theta z,amp}$= ±12 kPa). Figure 10 shows the shear modulus ($G_{\theta z}$) normalized by the void radio function $F(e) = e^{-1.10}$ to account for any sample volume change measured during the test. The investigation points were performed between the unloading-reloading loops (dotted line in Figure 10). For each cycle batch (B_i in Figure 10) the initial measurement ($G_{\theta z,i}$) is indicated with a right-pointing triangle marker while the consecutive values are indicated with square ones. The shear modulus evolution shows a consistent pattern: the initial stiffness built-up, measured after each monotonic loading/reloading, drops with the application of the first few thousand torsional cycles. Afterwards, the small strain stiffness seems to maintain the value for remaining cycles of the stage (Figure 10). The stiffness plateau value is analogous between the different sets of cyclic loading batches and similar results were observed for Young's modulus measurements.

This effect was further examined in *M00C45/90* (second half) and in *M00C45H*. Several cycle batches were performed at $\tau_{\theta z,amp}$ ranging from ±3, ±5, ±12 kPa to assess the influence of the loading amplitude on the magnitude and rate of the stiffness drops (Figure 11). As expected, the effect was found largely dependent on the amplitude of the cycle applied. While for $\tau_{\theta z,amp}$ = ±3 kPa the stiffness change ($G_{\theta z}/G_{\theta z,i}$) is contained within 3.5%, for $\tau_{\theta z,amp}$=±5 kPa the decay of shear modulus was up to 11%. The largest drop (18%) was observed for the largest cyclic amplitudes $\tau_{\theta z,amp}$=±12 (Figure 11).

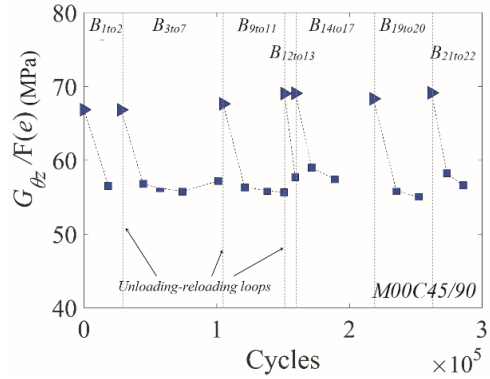

Figure 10 Change of $G_{\theta z}/F(e)$ with the number of cycles for test M00C45/90

The deviatoric stress level was found to only marginally affect the loss of stiffness with torsional loading. The change in shear modulus ratios ($G_{\theta z}/G_{\theta z,i}$) for cyclic loading carried out at q_{ave1} were found 5% larger than the ones produced at higher stress level.

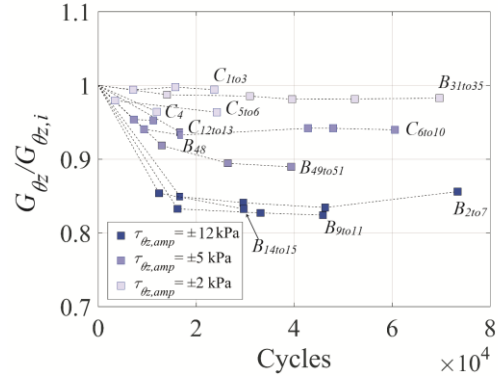

Figure 11 Evolution of shear modulus ratio with the number of cycles

The influence of the cyclic loading directions ($\alpha_{\sigma,c}$) was investigated in test *M00C45/90* (Figure 11). In case of compressional/extension cycle batches, the sample was found to conserve the

stiffness measured after the monotonic loading-reloading loops. However, in the case of $\alpha_{\sigma,m} \neq \alpha_{\sigma,c}$, the stiffness build-up can drop dramatically within the first $1 \cdot 10^4$ to $2 \cdot 10^4$ torsional cycles (Figure 12).

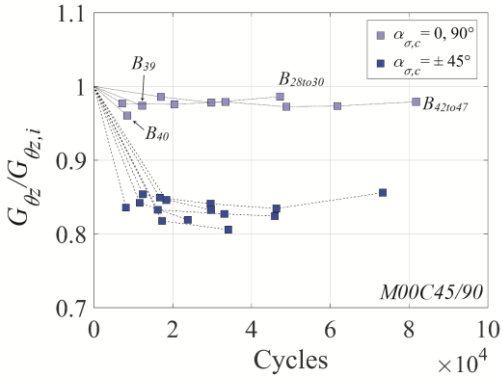

Figure 12 Evolution of shear modulus ratio with the number of cycles, $\alpha_{\sigma,c}$ influence.

9 CONCLUSIONS

Using FE analysis, this work has demonstrated that soil elements around a laterally loaded pile are subjected to complex rotation of principal stress axes. The HCTA permits such rotation to be imposed during soil element testing. The performed testing programme has focused on a soil element in front of the pile which may be initially consolidated in similar to triaxial compression conditions and then subject to a high number of cyclic loading with different orientation of principal stress axes.

Application of low-amplitude torsional cyclic loading causes a decrease in soil shear stiffness. A stabilised value of stiffness was reached after the application of first $1.0\text{-}2.0 \cdot 10^4$ cyclic loading. This plateau did not seem to change as the tests proceeded. The magnitude of the drops reached up to 18% of the initial stiffness measurements and it was dependent on the magnitude of the torsional cyclic loading. Conversely, no or very limited drop of stiffness was found when the direction of pre- and cyclic loading coincided, suggesting that the re-orientation of principal stress axes has a major effect on the evolution of soil stiffness. For both cases, the soil stiffness was reinstated after the application of large unloading-reloading cycles.

These results show that the soil conditions may change after long-term cyclic loading and, since OWT are dynamically sensitive structure, such effects may need to be carefully considered if more optimised and less conservative foundation design is pursued in future offshore developments.

10 REFERENCES

Abdel-Rahman, K. & Achmus, M., 2005. Finite element modelling of horizontally loaded monopile foundations for offshore wind energy converters in Germany. *Frontiers in Offshore Geotechnics*. Taylor & Francis

Achmus, M., Kuo, Y.-S. & Abdel-Rahman, K., 2009. Behavior of monopile foundations under cyclic lateral load. *Computers and Geotechnics*, 36(5), pp.725–735.

EWEA, 2015, Wind energy scenarios for 2030, a report by the European Wind Energy Association.

Hight, D.W., Gens, A., Symes, M.J. 1983. The development of a new hollow cylinder apparatus for investigating effects of principal stress rotation in soils. *Géotechnique* 33(4), 355-383.

LeBlanc, C., 2009. Design of Offshore Wind Turbine Support Structures. *PhD thesis*. Aalborg University.

Mandolini, A., Diambra, A., Ibraim, E. 2018. Strength anisotropy of fibre-reinforced sands under multiaxial loading. *Géotechnique*, 1-14. https://doi.org/10.1680/jgeot.17.P.102

Nikitas, G., Vimalan, N. & Bhattacharya, S., 2016. An innovative cyclic loading device to study long term performance of offshore wind turbines. *Soil Dynamics and Earthquake Engineering*, 82, pp.154–160.